93-275

Robustness Analysis and Control System Design for a Hydraulic Servo System

Yi Cheng and Bart L. R. De Moor, *Senior Member, IEEE*

Abstract—**In this paper, we treat the robustness analysis and control system design for the hydraulic servo system in a continuously variable transmission (CVT). The hydraulic system is subject to many uncertainties because of linearization, changes in temperature and errors in specified data. All these uncertainties are modeled in bounded and structured form, and the system is represented by a linear fractional transformation such that singular value and μ analysis and design methods can be used. Four control designs are proposed: classical PID control, H_∞ (sub)optimal control, μ synthesis with D–K iteration, μ synthesis with PID parameter search. For each of them, the robustness of stability and performance is analyzed with singular value and μ tests. The results confirm that the singular value test may be conservative compared to the μ test. When, for this specific control system, the μ analysis method is combined with a PID control structure, it can be guaranteed that the stability and performance robustness are satisfied and the control structure is as simple as a PID controller. Simulations are made for all the control designs.**

I. Introduction

A CONTINUOUSLY VARIABLE transmission (CVT) scheme is shown in Fig. 1. The specific CVT-part is a pair of steel V-shaped pulleys (primary and secondary pulleys) connected by a steel belt which is used to transfer torque between the pulleys. Each pulley consists of one fixed sheave (the left one for the secondary pulley) and one axially slidable sheave (the right one for the secondary pulley). The two moving sheaves are connected to two corresponding hydraulic cylinders/pistons. The engine shift is coupled, through a multiplate wet clutch with the primary pulley. The secondary pulley finally is connected to the vehicle wheel. Clearly the positions of the slidable sheaves, which determine the transmission ratio, and the clipping force on the belt, which determines the maximum torque to be transferred, are determined by the pressures on the slidable sheaves of the pulleys (p^{sc}, for the secondary pulley). The ultimate goal is to design an electronic control system for the CVT such that some performance specifications for vehicles (such as comfortable driver feeling, lower fuel consumption, small acceleration

Manuscript received February 8, 1994. This work was supported by Volvo Car Sint-Truiden (VCST), the Flemish Institute for Scientific and Technological Research in Industry (IWT) and the Belgian program on interuniversity attraction poles (IUAP-17 & IUAP-50) initiated by the Belgian State—Prime Minister's Office—Science Policy Programming. Paper recommended by Associate Editor J. Winkelman.

C. Yi is with the Department of Electrical Engineering, Katholieke Universiteit Leuven, B-3001, Heverlee, Belgium.

B. L. R. De Moor is with the Department of Electrical Engineering, Katholieke Universiteit Leuven, B-3001, Heverlee, Belgium and with the NFWO (Belgian National Fund for Scientific Research).

IEEE Log Number 9403392.

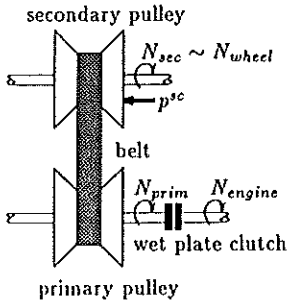

Fig. 1. A CVT scheme.

time) can be satisfied. The control system is divided up into two levels. The upper level control system determines the required hydraulic signals (p^{sc}, for instance). The lower level control system controls the hydraulic servo system. Here we only design a part of the low level control system to control the secondary cylinder pressure p^{sc}.

The hydraulic circuit, which generates p^{sc}, is shown in Fig. 2 together with the symbols that will be used to describe its components, where G_{r1}^{sv}, G_{r2}^{sv}, G_{r3}^{sv} and G_r^{sc} denote hydraulic resistors; C_{c1}^{sv}, C_{c2}^{sv}, C_c^{sc} and C_c^{ch} denote hydraulic capacitors; I_m^{sc} and I_m^{sv} denote mechanical inductors or translational objects (here the pistons); C_k^{sv} and C_k^{sc} denote the mechanical capacitors or linear massless springs; and R_f^{sc}, R_f^{sv} denote sliding friction resistors. The secondary circuit consists of one valve and one cylinder connected with a channel. The inputs to it are the oil flow q^{sv} from the oil pump driven by the engine with rotation speed N_{engine}, the force f_1^{sc} from the primary cylinder (not shown in Fig. 2), the clutch pressure p^{cl} and the servo pressure p_1^{sv} from the controller. The only output is the secondary pressure p^{sc} in the secondary cylinder, which is the variable to be controlled, assuming that q^{sv} and p^{cl} are constant and the piston in the secondary cylinder is fixed (but its position remains unknown). We then have a SISO system with the servo pressure p_1^{sv} as the input and the secondary pressure p^{sc} as the output. The process operates as follows: when the servo pressure p_1^{sv} is high, the piston I_m^{sv} in the valve will move towards the left, making a larger opening of the valve or a smaller resistance of the opening, consequently the pressure in the channel is lower, resulting in a lower pressure p^{sc} in the cylinder. When the servo pressure p_1^{sv} is low, the result is just opposite. So we can control the secondary pressure p^{sc} via the servo pressure p_1^{sv}. The actuator, which transfers electrical servo signal (from controller) into hydraulic servo pressure p_1^{sv}, is a pulse width modulated (PWM) valve. The PWM frequency is high, compared to the bandwidth of

1063-6536/94$04.00 © 1994 IEEE

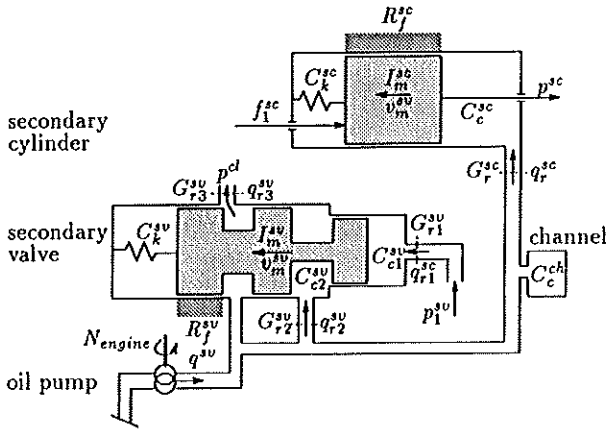

Fig. 2. The secondary valve hydraulic circuit of CVT.

the hydraulic system. The dynamics of the PWM valve is neglected. The dynamics of the pressure sensor is also omitted as its response time is small (< 1 ms).

To model the process, all components (resistors, capacitors, and inductors) are modeled by input/output function blocks based on hydraulic and mechanical laws. The global process is modeled with block diagrams by connecting all these blocks via the bond graph method [1]. All the block diagrams are put in the MATRIX$_X$ Super Block format [2]. In the process of doing so, one is confronted with the following uncertainties:

The Uncertainty of the Temperature: The hydraulic resistance is a function of the oil density (ρ) and viscosity (ν). Both oil density and viscosity change with the temperature, so does the resistance. As the temperature often changes from time to time, it may be quite different at the starting point and at the normal working point. However, the resistance change caused by the temperature is certainly bounded, for the temperature change is always bounded.

The Uncertainty of the Specified Design Data: All of the components (resistors, capacitors, and inductors) are modeled based on specified design data. These specified design data however are not always so accurate. For example, the compliance of the spring can be different from the specified design because of the possible variance in the production procedure. Again, this uncertainty is bounded and can be provided by the manufacture factory. The uncertainty of the constant capacitance of C_c^{sc} belongs to this class of uncertainties, as the volume of it is unknown but bounded.

The Nonlinearities: As we see from Fig. 2, the hydraulic capacitors (C_{c2}^{sv} and C_{c1}^{sv}) are time varying as the volumes of the corresponding cylinders change with the piston's position so the capacitances are variable; further more, all the hydraulic resistors (G_{r1}^{sv}, G_{r2}^{sv}, G_{r3}^{sv} and G_r^{sc}) and the slipping friction resistor (R_f^{sv}) are nonlinear. To design a controller with methods for linear systems, we use some linear models for these component functions. The errors of the models are bounded for the time varying components (here the capacitors) because the working ranges for these components are actually limited. For example, the volumes of the cylinders are limited, so are the corresponding hydraulic capacitances. For the nonlinear components (here the resistors), the errors of models can be unbounded or too large theoretically. In this case, we make some assumptions on the bounds and check the results by simulation afterwards.

In this paper we analyze and design the robust control system for the secondary hydraulic circuit of the continuously variable transmission we have just described and which is subject to the uncertainties described above. At first, all these uncertainties are modeled in bounded and structured form, and the system is represented by a linear fractional transformation (LFT) such that singular value and μ analysis and design methods can be used. Four control designs are proposed: classical PID control, H_∞ (sub)optimal control, μ synthesis with D–K iteration, μ synthesis with PID parameter search. For each of them, the robustness of stability and performance is analyzed with singular value and μ tests. The paper is organized as follows. After giving some notation at the end of this section, we will show, in Section II, two general procedures to model norm-bounded perturbations. With these methods, uncertainties from hydraulic resistors and capacitors are modeled in Section III by giving some typical examples. Section IV gives the performance specification and the open loop interconnection. Section V will describe and compare all the results from the different analysis and design methods. Some conclusions are made in Section VI. In the appendix, brief descriptions of robust analysis and synthesis methods are given: automatic PID control tuning, μ test and μ synthesis, namely D–K iteration. In addition, to overcome the disadvantage of the controller being of high order in the D–K iteration, a local search for PID controller parameters such that the maximum μ is smaller than 1 is also introduced in the appendix.

A. Notation

LFT: Suppose M is a matrix partitioned as

$$M = \begin{bmatrix} M_{11} & M_{12} \\ M_{21} & M_{22} \end{bmatrix} \in C^{(p_1+p_2)\times(q_1+q_2)}$$

and let $\Delta_1 \subset C^{q_1 \times p_1}$ and $\Delta_2 \subset C^{q_2 \times p_2}$, the LFT is defined as a matrix function

$$F_u(M, \Delta_u) = M_{22} + M_{21}\Delta_u(I - M_{11}\Delta_u)^{-1}M_{12}$$

or

$$F_l(M, \Delta_l) = M_{11} + M_{12}\Delta_l(I - M_{22}\Delta_l)^{-1}M_{21}$$

for some $\Delta_u \in \Delta_1$ and $\Delta_l \in \Delta_2$, provided that the inverses exist. $F_u(M, \Delta_u)$ and $F_l(M, \Delta_l)$ are called upper and lower LFT's with respect to the parameter matrices Δ_u and Δ_l respectively, and matrix M is called the coefficient matrix. The LFT is a general concept which is used in uncertainty modeling and robustness analysis and control synthesis, typically with the μ method.

$\bar{\sigma}(M)$: Maximum singular value of matrix $M \in C^{p\times q}$.
$\mu_\Delta(M)$: Structured singular value of matrix $M \in C^{n\times n}$ with respect to the block structure Δ, see Appendix-B for

details of the definition of μ. $\|G_c\|_\infty$: H_∞ norm of the closed loop transfer function G_c:

$$\|G_c\|_\infty = \sup_{\omega\in\mathcal{R}}\{\bar{\sigma}(G_c(j\omega))\}.$$

$\|G_c\|_\Delta$: Maximum structured singular value of the closed loop transfer function over all frequencies:

$$\|G_c\|_\Delta := \sup_{\omega\in\mathcal{R}}\{\mu_\Delta(G(j\omega))\}.$$

II. Norm Bounded Structured Uncertainty Modeling

A. System Modeling and Uncertainty Modeling

The system here consists of several mechanical, hydraulic subparts, and even electrical subparts if we consider the actuators. For such a complex system, the bond graph technique [3] is used for system modeling. When constructing a bond graph model, one can split up two different aspects: Creating a bond graph gives form to the modeling phase to obtain a true representation of the physical dynamic system; analysis of the computational causality of the bond graph will result in a computable form of the model. In constructing a bond graph, the main concern will be the calculation of the average volume of flow rates through orifices and pressures in the hydraulic subsystem, and the macro fluid dynamic interaction with the solid mechanical elements (valves, cylinders, ...). Under these approximations an exact bond graph representation is not necessary, and the familiar lumped parameter model is used because the hydraulic subsystem is in fact a servo mechanism for which the volume flow rates are rather low and the high order dynamics of the hydraulic inertia can be neglected.

We used the software package MATRIX$_X$ [2] for modeling and simulation and MATLAB [4] for robust analysis and control design. But the input data for MATRIX$_X$ or MATLAB must consist of (causal) block diagrams or alike-structure, not a bond graph. The conversion of a bond graph to a block diagram is thus necessary. We are not going to show how these block diagrams were constructed, but refer to [1] for more details.

For robustness analysis and control design by the singular value test/H_∞ synthesis or μ test/synthesis, the first step which has to be taken is to extract all uncertainties out of the process model, such that the process model can be described with a LFT as shown in Fig. 3, where w_d is the exogenous signal vector (references and disturbances etc.), u is the control input vector; w_δ is the uncertainty output vector; z_e is the regulated output vector, y is the measured signal vector and z_δ is the uncertainty input vector; $P(s)$ is the plant transfer function from w_d and u to z_e and y with some uncertainties; $M(s)$ is a transfer function from $w := [w_\delta^t\ w_d^t]^t$ and u to $z := [z_\delta^t\ z_e^t]^t$ and y, and $\Delta(s)$ is the uncertainty transfer function (or operator in nonlinear case). For unstructured, bounded uncertainties, $\Delta(s) \in \mathcal{C}^{n_{w_\delta}\times n_{z_\delta}}$, $\forall s \in \mathcal{C}$, n_{w_δ} and n_{z_δ} being the dimensions of the vectors w_δ and z_δ respectively. For structured bounded uncertainties, $\Delta(s) \in \mathbf{\Delta} \subset \mathcal{C}^{n\times n}$(here for simplicity $n_w = n_z = n$), $\forall s \in \mathcal{C}$. $\mathbf{\Delta}$ is the set with some specific structure described by a block structure vector bs (see the definition of μ in Appendix-B). By scaling, we can always have $\|\Delta(s)\|_\infty \le 1$ (Δ is non-expansive in nonlinear case). The general philosophy of modeling uncertainty with LFT's is often referred to as "pulling out the Δs" [5]. Here we introduce two procedures of uncertainty modeling for the systems described by block diagrams and for the systems described by transfer functions.

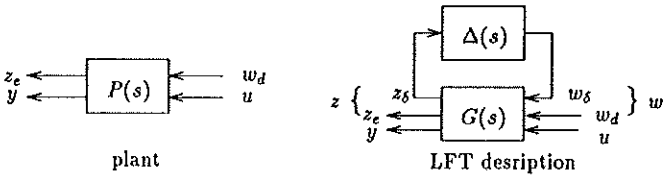

Fig. 3. Extracting uncertainties from the plant by a LFT.

B. Modeling Complex Valued Norm Bounded Uncertainties Based on System Block Diagrams

One way to get the matrix M and the block structure matrix bs is to first represent the system with an interconnection of the transfer block diagrams, for example, the Super Blocks in MATRIX$_X$. Then, we merely cut off the uncertainty blocks (Δs) from the interconnection, and define all inputs to these Δs as new outputs of the remaining interconnection, all outputs from the Δs as new inputs of the remaining interconnection, and finally calculate the transfer matrix of the remaining interconnection. If some $\|\Delta_i\|_\infty > 1$, then it should be scaled such that $\|\Delta_i\|_\infty \le 1$. The procedure of modeling complex valued norm bounded uncertainties based on the system block diagrams can be summarized as follows:

1) Describe the uncertainties using norm bounded input/output models (blocks Δ_i) for all uncertainty blocks.
2) Scale all these uncertainty blocks such that each $\|\Delta_i\|_\infty \le 1$.
3) Cut off all of these uncertainty blocks from the original block diagram. What remains is the nominal system. Get the block structure matrix bs from these uncertainty blocks.
4) Label all inputs to the uncertainty blocks as additional outputs of the nominal system, and all outputs from the uncertainty blocks as additional inputs of the nominal system.
5) Get the transfer matrix M from the remaining nominal system block diagram.

Remark that Step 1 and Step 2 includes linearization procedures for the nonlinear blocks. This procedure is extremely easy when using MATRIX$_X$, where the last step can be done by the command "lin".

C. Parameter Uncertainty Modeling Based on Transfer Functions

There is another typical way to solve parametric uncertainty modeling problems when the systems are represented by a transfer function matrix $P(p)$ with each entry being a rational function of the uncertainty parameter vector p. The procedure for the parametric uncertainty modeling can be summarized as follows:

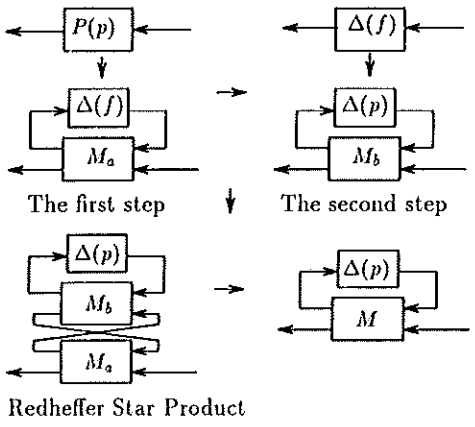

Fig. 4. Description of the two step realization algorithm. $P(p)$ is the plant with parametric uncertainties. In the first step, $P(p)$ is realized as a LFT with a diagonal rational $\Delta(f)$. $\Delta(f)$ is then realized in the second step as a LFT with a block diagonal $\Delta(p)$. The two realizations are then "cascaded" via a Redheffer Star product.

1) Obtain lower and upper bounds of uncertainty parameters p_i.
2) Scale all these uncertainty parameters such that each $|p_i| \leq 1$.
3) Rewrite the transfer function matrix in the form $P(p) = P_{nom} + \sum_{i=1}^{l} f_i(p)P_i$, with $f_i(p)$ being a rational function of the vector p and $f_i(0) = 0$.
4) Get the transfer function matrix M and block structure matrix bs for the LFT.

The last step of the procedure is actually the multidimensional realization problem, which we have described in detail in [6]. The main idea of the algorithm described there is to realize the affine part of the rational matrix at first, then the rational function part in the second step. The two realizations are finally "cascaded" via the Redheffer Star Product as shown in Fig. 4.

III. Modeling the Uncertainties of the Hydraulic Circuit of CVT

As the secondary hydraulic circuit is already modeled with block diagrams, we use the method in Section II-B to model the uncertainties. We assume that the design data are correct, so the uncertainties are from the linearization errors and the temperature changes. The capacitance of C_c^{sc} is constant but its value is unknown. The capacitances of C_{c1}^{sv} and C_{c2}^{sv} are variable. The capacitances of C_c^{ch} and C_k^{sv} are known and constant. All the hydraulic resistors are nonlinear. The sliding resistance of R_f^{sv} is rather small and assumed to be linear as a function of velocity. So uncertainty modeling is needed for all variable or unknown capacitors and hydraulic resistors. The uncertainty modeling procedures for all the capacitors C_c^{sc}, C_{c1}^{sc} and C_{c2}^{sc} are similar, and the uncertainty modeling procedures are also similar for the resistors G_r^{sc}, G_{r1}^{sv} and G_{r2}^{sv}. So in what follows, we will only show the modeling procedures for the capacitor C_c^{sc}, the resistors G_r^{sc} and G_{r3}^{sv}.

Uncertainty Modeling for C_c^{sc}: We redraw the Super Block diagram of C_c^{sc} in Fig. 5(a), where the dashed box represents the inverse of the capacitance. The uncertainty modeling procedure is described in the following steps, which are illustrated in Fig. 5(b)–(d):

Step 1 (Fig. 5(a) and (b)): Calculate the maximum and minimum values of the inverse of the capacitance in the dashed box. This is easy as we know that the maximum and minimum volumes of the cylinder are 400 and 158 ml respectively and the bulk modulus of the oil is 4×10^3 (bar) from the design specification, so

$$(\frac{1}{C})_{\max} = \frac{4 \times 10^3}{158}(\text{bar/ml}^3)$$

$$(\frac{1}{C})_{\min} = \frac{4 \times 10^3}{400}(\text{bar/ml}^3).$$

Step 2 (Fig. 5(c)): Scale the uncertainty. The uncertainty is scaled [7] such that

$$(\frac{1}{C}) = (\frac{1}{C})_n + (\frac{1}{C})_s \Delta_c$$

$$\|\Delta_c\| \leq 1$$

where $(\frac{1}{C})_n$ and $(\frac{1}{C})_s$ are the nominal value and the scaling factor respectively and

$$(\frac{1}{C})_n = \frac{(\frac{1}{C})_{\max} + (\frac{1}{C})_{\min}}{2} = 17.7(\text{bar/ml}^3)$$

$$(\frac{1}{C})_s = \frac{(\frac{1}{C})_{\max} - (\frac{1}{C})_{\min}}{2} = 7.66(\text{bar/ml}^3).$$

Step 3 (Fig. 5(d)): Cut the uncertainty block off from the system, and introduce a new input w_{csc} and a new output z_{csc}.

Uncertainty modeling for G_r^{sc}: We use the admittance g of a resistor which is defined

$$g = \frac{q}{p} \text{ so } q = gp$$

where p is the pressure and q is the flow. The relation between input pressure p and output flow q for resistor G_r^{sc} is described by [1]

$$q = \min(0.611; \sqrt{\frac{0.611^3 D_h}{20\nu(T)}\sqrt{\frac{2p}{\rho(T)}}})a_r\sqrt{\frac{2p}{\rho(T)}} \quad (1)$$

where D_h is a constant depending on the geometry of the channel, a_r is the cross section area of the channel and $\nu(T)$ and $\rho(T)$ are oil viscosity and density respectively. The uncertainty modeling procedure for G_r^{sc} is exactly the same as that for C_c^{sc}, except that the first step is not so trivial. The output flow q is not only a function of the oil density and viscosity, which themselves are functions of the temperature T, but it is also a complicated function of the input p. We already knew that the pressure p on G_r^{sc} is in the range $|p| < 40$ bar, the temperature is in the range $-20°\text{ C} < T < 130°\text{ C}$ in practice and oil density $\rho(T)$ and

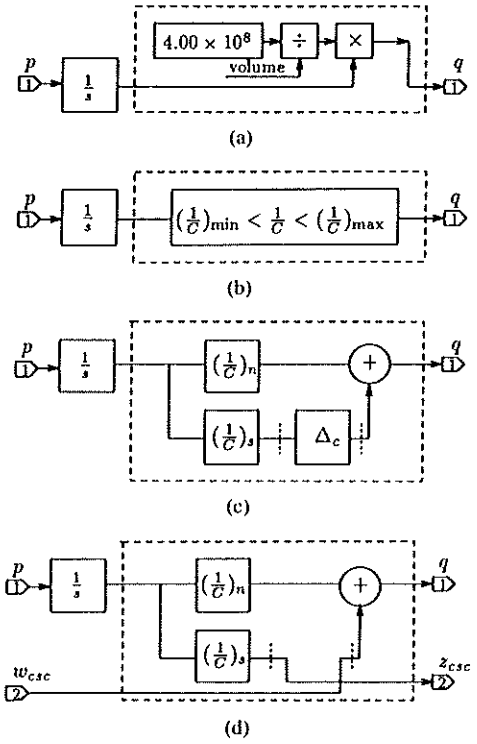

Fig. 5. Uncertainty modeling of C_c^{sc}. (a) gives the original model, the maximum and minimum values of the capacitance is evaluated in (b). (c) introduces a normal value and scales uncertainty. The uncertainty block is cut off and a new input and a new output is defined in (d). The inputs and outputs are indexed in connection pins.

viscosity $\nu(T)$ are monotonically decreasing functions of the temperature T as shown in Fig. 6. With (1) we easily find:

$$g_{max} = \left.\frac{q}{p}\right|_{p=0(\text{bar}),\ T=130^\circ\ \text{C}}$$

$$g_{min} = \left.\frac{q}{p}\right|_{p=40(\text{bar}),\ T=-20^\circ\ \text{C}}.$$

But when $p = 0$, g is not well defined as it goes to infinity. Therefore we assume that the minimum pressure p is 2.5 bar, which is equivalent to assume that g is constant when $p < 2.5$. This assumption is reasonable as when the pressure p is low, the flow q will be proportional to the pressure p and g will be constant. D_h is 0.01 from the specification, then we have:

$$g_{max} = \left.\frac{q}{p}\right|_{p=2.5(\text{bar}),\ T=130^\circ\ \text{C}} \simeq 500(\text{ml}^3 \cdot \text{s/bar})$$

$$g_{min} = \left.\frac{q}{p}\right|_{p=40(\text{bar}),\ T=-20^\circ\ \text{C}} \simeq 100(\text{ml}^3 \cdot \text{s/bar})$$

The remaining steps of uncertainty modeling are the same as those for C_c^{sc}, and we obtain the block diagram in Fig. 7.

Uncertainty Modeling of G_{r3}^{sc}: The pressure and flow relation for resistor G_{r3}^{sc} is similar to (1), but with

$$a_r = a_r(x);\ D_h = \sqrt{\frac{4}{\pi} a_r(x)} \tag{2}$$

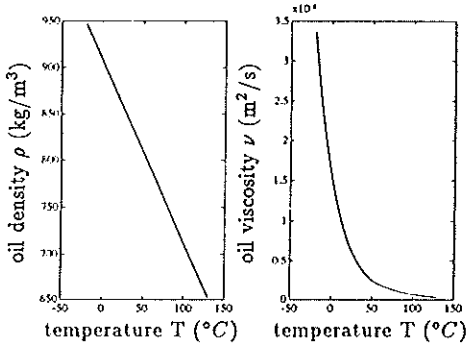

Fig. 6. Oil density $\rho(T)$ and viscosity $\nu(T)$.

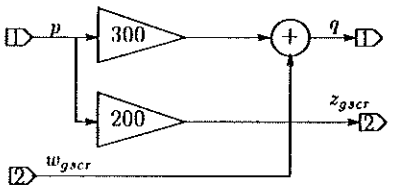

Fig. 7. Block diagram for G_r^{sc} with the uncertainty extracted. Compared to Fig. 5(d), 300 is the nominal value, 200 is the scaling factor.

where x is the piston position and the function $a_r(x)$ is nonlinear as shown in Fig. 8. Now we write q as:

$$q = (\lambda \frac{q}{x})x + ((1-\lambda)\frac{q}{p})p \tag{3}$$

where $0 < \lambda < 1$. Let

$$g_x = \lambda \frac{q}{x},\ \ g_p = (1-\lambda)\frac{q}{p}. \tag{4}$$

Then (3) becomes:

$$q = g_x x + g_p p. \tag{5}$$

Next we try to find the ranges for g_x and g_p. Simulations show that

$$0.01\ (\text{m}) < x < 0.02\ (\text{m});\ 2\ (\text{bar}) < p < 32\ (\text{bar}). \tag{6}$$

We choose $\lambda = 13/14$[1]. With (1), (2), (4), (6), and the opening function in Fig. 8, recalling that $\nu(T)$ and $\rho(T)$ are monotonic to T and choosing $x = 0.0162$ (m) at which $a_r(x)/x$ reaches

[1]The reason for this choice is as follows: Obviously we can choose any value in [0 1] for λ. Different λ values will lead to different g_x and g_p. But for robust analysis and control design, we need to choose the value such that the results are the least conservative. Actually we choose λ such that a μ synthesis based control design, satisfying the robustness and performance specification, is feasible. (Experience has shown that μ synthesis is not possible for all values of λ.)

its maximum, we can easily obtain

$$g_{xmax} = \left.\frac{13q}{14x}\right|_{p=32(\text{bar}),\ T=130(^\circ C),\ x=0.0162(\text{m})} = 7.5 \times 10^5(\text{ml}^3/\text{s/m})$$

$$g_{xmin} = \left.\frac{13q}{14x}\right|_{p=2(\text{bar}),\ T=-20(^\circ C),\ x=0.01(\text{m})} = 0$$

$$g_{pmax} = \left.\frac{q}{14p}\right|_{p=2(\text{bar}),\ T=130(^\circ C),\ x=0.02(\text{m})} == 120(\text{ml}^3/\text{s/bar})$$

$$g_{pmin} = \left.\frac{q}{14p}\right|_{p=32(\text{bar}),\ T=-20(^\circ C),\ x=0.01(\text{m})} = 0.$$

However, this uncertainty modeling is very conservative. Indeed, there is no controller at all which stabilizes the system in the "worst case": $g_{xmin} = 0$ and $g_{pmin} = 0$ when the relation of input x and p and output q of G_{r3}^{sv} is described by (5) linearly. This is easy to see by inspection from the layout of the secondary hydraulic circuit in Fig. 2: the "worst case" of $g_{xmin} = 0$ and $g_{pmin} = 0$ means that there is no flow passing through G_{r3}^{sv} at any time. As q^{sv} is constant, the pressure in the secondary cylinder will go to infinity whatever the input pressure p_1^{sv} is. The problem here is that we are not only dealing with uncertainties from changing temperature, but also the errors from linearization, which are dependent on the system variables. To eliminate the conservativeness, g_{xmin} and g_{pmin} have to be increased, here we choose:

$$g_{xmin} = \frac{g_{xmax}}{3} = 2.5 \times 10^5(\text{ml}^3/\text{s/m})$$

$$g_{pmin} = \frac{g_{pmax}}{3} = 40(\text{ml}^3/\text{s/bar}).$$

These assumptions mean that the secondary valve is never completely closed, and $x > 0.013$ (m). Although in steady state, these assumptions are true as the oil flow q^{sv} is assumed to be constant, dynamically, they do not always hold. Thus we need to check the results by closed loop simulation afterwards[2]. The remaining steps of the uncertainty modeling are the same as for C_c^{sc}, and the final result is shown in Fig. 9.

The Final Interconnection: As all possible components with uncertainties are modeled by a linear system with some new inputs and outputs for the uncertainties, we can easily get the final interconnection scheme shown in Fig. 10 in Super Block format. Note that the inputs and outputs with number 1 to 8 are the outputs and inputs pairs for the uncertainties in the components described above respectively, see Table I. Only the last input and the last output are the system input and output. Each (real) uncertainty is connected to a corresponding input/output pair. The system transfer function M of the secondary hydraulic circuit now can be easily

[2]Here we choose g_{xmin} and g_{pmin} again in the control design phase as we did for λ, see footnote 1. However, unlike λ, g_{xmin} and g_{pmin} are no longer the true value (0,0). So robustness can not be sufficiently guaranteed in the control design phase. We can only check the results by simulation afterwards. We recognize that this is a disadvantage of using analysis and synthesis methods for linear systems with bounded uncertainties to nonlinear uncertainty systems by taking nonlinearities as uncertainties when the nonlinearities are really large or even unbounded.

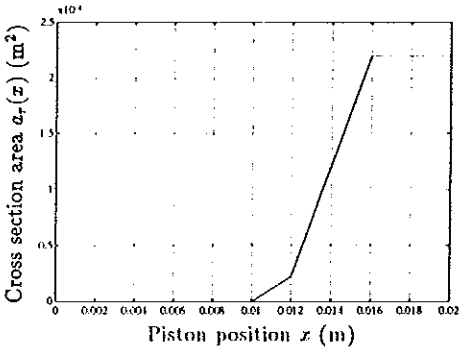

Fig. 8. The opening function $a_r(x)$ of G_{r3}^{sv} as a function of the piston position x.

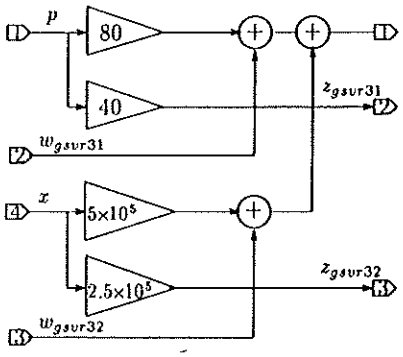

Fig. 9. Super Block diagram of G_{r3}^{sv} with uncertainty extracted. 80 and 5×10^5 are the nominal values of g_p and g_x respectively, 40 and 2.5×10^5 are the corresponding scaling factors.

obtained from the interconnection in Super Block form. The following is the state space realization of $M(s)$,

$$M(s) = \left[\begin{array}{c|c} A_m & B_m \\ \hline C_m & D_m \end{array}\right]$$

where (see the matrices at the bottom of the next page.)

For this realization, the corresponding states represent some physical quantities shown in Table II. As there are only scalar uncertainties, the block structure matrix (see Appendix-B for full details of a block structure) is

$$bs = \begin{bmatrix} 1 & 0 \\ 1 & 0 \\ 1 & 0 \\ 1 & 0 \\ 1 & 0 \\ 1 & 0 \\ 1 & 0 \\ 1 & 0 \end{bmatrix}.$$

IV. Performance Specification and Open Loop Interconnection

The secondary hydraulic circuit of the CVT is designed as a servo system: the output, the secondary pressure p^{sc}, is to track a reference or command signal w_d. So the control problem for the secondary circuit is a tracking problem. Hence one can translate the performance specification as the requirement that the H_∞ norm from the reference input w_d to the tracking

TABLE I
COMPONENTS AND CORRESPONDING UNCERTAINTY INPUT/OUTPUT PAIRS

Components	Label	
	input	output
G_{r1}^{sv}	w_{gsvr1}	z_{gsvr1}
G_{r2}^{sv}	w_{gsvr2}	z_{gsvr2}
G_{r3}^{sv}	w_{gsvr31}	z_{gsvr31}
	w_{gsvr32}	z_{gsvr32}
C_{c1}^{sv}	w_{csvc1}	z_{csvc1}
C_{c2}^{sv}	w_{csvc2}	z_{csvc2}
G_r^{sc}	w_{gscr}	z_{gscr}
C_c^{sc}	w_{csvc}	z_{csvc}

TABLE II
STATES AND CORRESPONDING PHYSICAL QUANTITIES

State No.	Name	In component	Description
1	v_m^{sv}	I_m^{sv}	velocity
2	x	I_m^{sv}	position
3	p_c^{ch}	C_c^{ch}	pressure
4	p_{c1}^{sv}	C_{c1}^{sv}	pressure
5	p_{c2}^{sv}	C_{c2}^{sv}	pressure
6	p^{sc}	C_c^{sc}	pressure

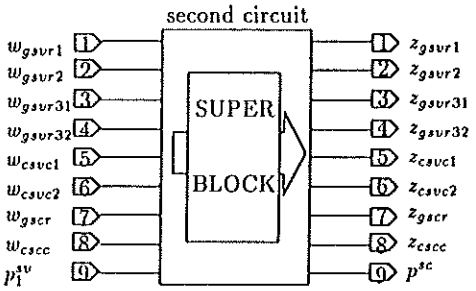

Fig. 10. Final interconnection in Super Block form.

error e between w_d and p^{sc} is less than some specified value. Here we use the frequency weighted H_∞ norm with a frequency weighting function W_p. The resulting open loop interconnection of the secondary circuit system together with the weighting function is shown in Fig. 11, where G is the open loop transfer function. The performance specification is:

$$\|F_u(G_c, \Delta)\|_\infty \leq 1 \tag{7}$$

where G_c is the closed loop (with a controller feedback from y to u) transfer function. Equation (7) shows that the

$$A_m = \begin{bmatrix} -1.3e3 & -2.1e3 & 0.0 & 8.0e3 & 9.0e3 & 0.0 \\ 5.3e1 & 0.0 & 0.0 & 0.0 & 0.0 & 0.0 \\ 0.0 & -8.0e4 & -2.6e4 & 0.0 & 1.8e4 & 3.0e2 \\ 7.5e3 & 0.0 & 0.0 & -1.7e4 & 0.0 & 0.0 \\ -8.0e2 & 0.0 & 2.0e2 & 0.0 & -1.8e4 & 0.0 \\ 0.0 & 0.0 & 3.5e5 & 0.0 & 0.0 & -5.3e3 \end{bmatrix}$$

$$B_m = \begin{bmatrix} 0.0 & 0.0 & 0.0 & 14.0 & 1.5 & 0.0 & 0.0 & 0.0 & 0.0 \\ 0.0 & 0.0 & 0.0 & 0.0 & 0.0 & 0.0 & 0.0 & 0.0 & 0.0 \\ 0.0 & -1.0 & -1.0 & 0.0 & 3.0 & -1.0 & 0.0 & -1.0 & 0.0 \\ 1.0 & 0.0 & 0.0 & -30.0 & 0.0 & 0.0 & 0.0 & 0.0 & 30.0 \\ 0.0 & 1.0 & 0.0 & 0.0 & -3.0 & 0.0 & 0.0 & 0.0 & 0.0 \\ 0.0 & 0.0 & 0.0 & 0.0 & 0.0 & 17.6 & 1.0 & 0.0 & 0.0 \end{bmatrix}$$

$$C_m = \begin{bmatrix} 0.0 & 0.0 & 0.0 & -5.7e3 & 0.0 & 0.0 \\ 0.0 & 0.0 & 1.3e2 & 0.0 & -1.2e4 & 0.0 \\ 0.0 & 0.0 & 2.7e3 & 0.0 & 0.0 & 0.0 \\ 0.0 & 0.0 & 0.0 & 6.1e1 & 0.0 & 0.0 \\ 0.0 & 0.0 & 0.0 & 0.0 & 7.1e2 & 0.0 \\ 0.0 & 0.0 & 1.3e4 & 0.0 & 0.0 & -2.0e2 \\ 0.0 & 0.0 & 1.5e5 & 0.0 & 0.0 & -2.3e3 \\ 0.0 & 4.0e4 & 0.0 & 0.0 & 0.0 & 0.0 \\ 0.0 & 0.0 & 0.0 & 0.0 & 0.0 & 1.0 \end{bmatrix}$$

$$D_m = \begin{bmatrix} 0.0 & 0.0 & 0.0 & -10.0 & 0.0 & 0.0 & 0.0 & 0.0 & 10.0 \\ 0.0 & 0.0 & 0.0 & 0.0 & -2.0 & 0.0 & 0.0 & 0.0 & 0.0 \\ 0.0 & 0.0 & 0.0 & 0.0 & 0.0 & 0.0 & 0.0 & 0.0 & 0.0 \\ 0.0 & 0.0 & 0.0 & 0.0 & 0.0 & 0.0 & 0.0 & 0.0 & 0.0 \\ 0.0 & 0.0 & 0.0 & 0.0 & 0.0 & 0.0 & 0.0 & 0.0 & 0.0 \\ 0.0 & 0.0 & 0.0 & 0.0 & 0.0 & 0.0 & 0.0 & 0.0 & 0.0 \\ 0.0 & 0.0 & 0.0 & 0.0 & 0.0 & 7.66 & 0.0 & 0.0 & 0.0 \\ 0.0 & 0.0 & 0.0 & 0.0 & 0.0 & 0.0 & 0.0 & 0.0 & 0.0 \\ 0.0 & 0.0 & 0.0 & 0.0 & 0.0 & 0.0 & 0.0 & 0.0 & 0.0 \end{bmatrix}.$$

maximum singular value curve of the closed loop transfer function $F_u(G_c, \Delta)(j\omega)W_p^{-1}$ from w_d to e is required to lie below the curve of $|W_p^{-1}(j\omega)|$ for any uncertainty $\Delta \in \mathbf{\Delta}$. We choose the weighting function as:

$$W_p(s) = 0.5\frac{s+30}{s+0.3}$$

the inverse of which has the magnitude of the frequency response curve shown in Fig. 12. It is easy to check that the ratio of the reference to tracking error in the steady state is less than 0.02. The zero of $W_p(s)$ is chosen such that the inverse of it $1/30 = 0.033$ is less than 0.05 second which is the specified rising time. The open loop transfer function G in Fig. 11 then has the following realization (see the matrices on this page):

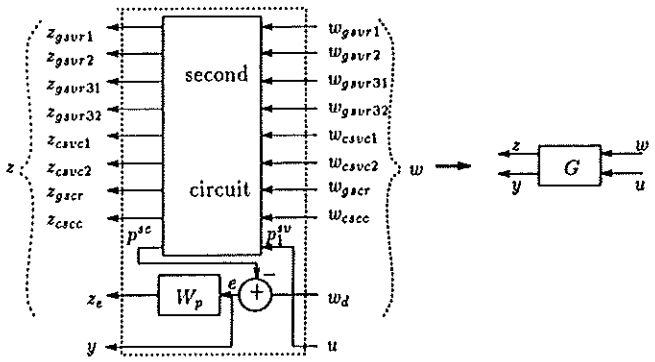

Fig. 11. Open loop interconnection structure.

$$A = \begin{bmatrix} -1.3e3 & -2.1e3 & 0.0 & 8.0e3 & 9.0e3 & 0.0 & 0.0 \\ 5.3e1 & 0.0 & 0.0 & 0.0 & 0.0 & 0.0 & 0.0 \\ 0.0 & -8.0e4 & -2.6e4 & 0.0 & 1.8e4 & 3.0e2 & 0.0 \\ -7.5e3 & 0.0 & 0.0 & -1.7e4 & 0.0 & 0.0 & 0.0 \\ -8.0e2 & 0.0 & 2.0e2 & 0.0 & -1.8e4 & 0.0 & 0.0 \\ 0.0 & 0.0 & 3.5e5 & 0.0 & 0.0 & -5.3e3 & 0.0 \\ 0.0 & 0.0 & 0.0 & 0.0 & 0.0 & -5.03-1 & -0.3 \end{bmatrix}$$

$$B = [B_w \quad B_u] = \left[\begin{array}{ccccccccc|c} 0.0 & 0.0 & 0.0 & 14.0 & 1.5 & 0.0 & 0.0 & 0.0 & 0.0 & 0.0 \\ 0.0 & 0.0 & 0.0 & 0.0 & 0.0 & 0.0 & 0.0 & 0.0 & 0.0 & 0.0 \\ 0.0 & -1.0 & -1.0 & 0.0 & 3.0 & -1.0 & 0.0 & -1.0 & 0.0 & 0.0 \\ 1.0 & 0.0 & 0.0 & -30.0 & 0.0 & 0.0 & 0.0 & 0.0 & 0.0 & 30.0 \\ 0.0 & 1.0 & 0.0 & 0.0 & -3.0 & 0.0 & 0.0 & 0.0 & 0.0 & 0.0 \\ 0.0 & 0.0 & 0.0 & 0.0 & 0.0 & 17.6 & 1.0 & 0.0 & 0.0 & 0.0 \\ 0.0 & 0.0 & 0.0 & 0.0 & 0.0 & 0.0 & 0.0 & 0.0 & 0.5 & 0.0 \end{array}\right]$$

$$C = \begin{bmatrix} C_z \\ C_y \end{bmatrix} = \left[\begin{array}{ccccccc} 0.0 & 0.0 & 0.0 & -5.7e3 & 0.0 & 0.0 & 0.0 \\ 0.0 & 0.0 & 1.3e2 & 0.0 & -1.2e4 & 0.0 & 0.0 \\ 0.0 & 0.0 & 2.7e3 & 0.0 & 0.0 & 0.0 & 0.0 \\ 0.0 & 0.0 & 0.0 & 6.1e1 & 0.0 & 0.0 & 0.0 \\ 0.0 & 0.0 & 0.0 & 0.0 & 7.1e2 & 0.0 & 0.0 \\ 0.0 & 0.0 & 1.3e4 & 0.0 & 0.0 & -2.0e2 & 0.0 \\ 0.0 & 0.0 & 1.5e5 & 0.0 & 0.0 & -2.3e3 & 0.0 \\ 0.0 & 4.0e4 & 0.0 & 0.0 & 0.0 & 0.0 & 0.0 \\ 0.0 & 0.0 & 0.0 & 0.0 & 0.0 & -5.0e-1 & 3.0e1 \\ \hline 0.0 & 0.0 & 0.0 & 0.0 & 0.0 & -1.0e0 & 0.0 \end{array}\right].$$

$$D = \begin{bmatrix} D_{zw} & D_{zu} \\ D_{yw} & D_{yu} \end{bmatrix} = \left[\begin{array}{ccccccccc|c} 0.0 & 0.0 & 0.0 & -10.0 & 0.0 & 0.0 & 0.0 & 0.0 & 0.0 & 10.0 \\ 0.0 & 0.0 & 0.0 & 0.0 & -2.0 & 0.0 & 0.0 & 0.0 & 0.0 & 0.0 \\ 0.0 & 0.0 & 0.0 & 0.0 & 0.0 & 0.0 & 0.0 & 0.0 & 0.0 & 0.0 \\ 0.0 & 0.0 & 0.0 & 0.0 & 0.0 & 0.0 & 0.0 & 0.0 & 0.0 & 0.0 \\ 0.0 & 0.0 & 0.0 & 0.0 & 0.0 & 0.0 & 0.0 & 0.0 & 0.0 & 0.0 \\ 0.0 & 0.0 & 0.0 & 0.0 & 0.0 & 0.0 & 0.0 & 0.0 & 0.0 & 0.0 \\ 0.0 & 0.0 & 0.0 & 0.0 & 0.0 & 7.7 & 0.0 & 0.0 & 0.0 & 0.0 \\ 0.0 & 0.0 & 0.0 & 0.0 & 0.0 & 0.0 & 0.0 & 0.0 & 0.0 & 0.0 \\ 0.0 & 0.0 & 0.0 & 0.0 & 0.0 & 0.0 & 0.0 & 0.0 & 0.5 & 0.0 \\ \hline 0.0 & 0.0 & 0.0 & 0.0 & 0.0 & 0.0 & 0.0 & 0.0 & 1.0 & 0.0 \end{array}\right]$$

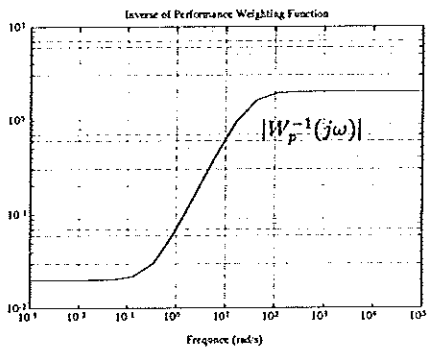

Fig. 12. Magnitude of the frequency response of W_p^{-1}.

Note that the seventh state (corresponding to last column and row of matrix A, the last row of matrix B and the last column of matrix C) is the state for weighting function $W_p(s)$; the ninth and tenth inputs are the command signal w_d and control input u (corresponding to ninth and tenth columns of matrix B and D); the ninth and tenth outputs are the tracking error z_e and measurement y (corresponding to the ninth and tenth rows of matrices C and D). The ninth input p_1^{sv} and output p^{sc} for the open loop system is eliminated. The block structure now is

$$bs = \begin{bmatrix} 1 & 0 \\ 1 & 0 \\ 1 & 0 \\ 1 & 0 \\ 1 & 0 \\ 1 & 0 \\ 1 & 0 \\ 1 & 0 \\ 1 & 1 \end{bmatrix}.$$

The last row of bs corresponds to the fictitious uncertainty block for the performance specification, see Appendix-B for detail.

V. Evaluation and Comparison

In this section we use different methods to design a controller for the open loop system G shown in Fig. 11, and use the singular value test and μ test for the stability and performance robustness analysis to the closed loop system G_c, shown in Fig. 13 where K is a controller, and $G_c = F_l(G, K)$. The closed loop system G_c includes the weighting function W_p. Based on the discussion in Appendix-B for robust stability and performance, we need, with the singular value test

$$\|G_c\|_\infty = \sup_{\omega \in \mathcal{R}} (\bar{\sigma}(G_c(j\omega))) < 1,$$

or with μ test

$$\|G_c\|_\Delta = \sup_{\omega \in \mathcal{R}} (\mu(G_c(j\omega))) < 1.$$

We used the MATLAB μ toolbox [4] for all the analysis and design.

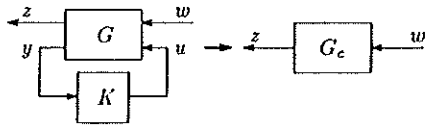

Fig. 13. The closed loop system G_c with a controller K.

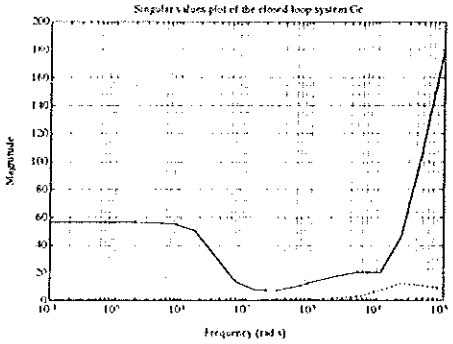

Fig. 14. Singular value plot of closed loop system G_c with PID controller K_{pid} with $K_p = -7.7143e-02$, $K_i = -5.7359e+00$, $K_d = -2.5976e-04$.

A. PID Control 1: Classical Tuning

The PID parameters were tuned on the original model (SISO nonlinear model), with the method described in Appendix-A. The hysteresis width h and the amplitude m of the relay tuner were set to 10 and 2.5 bar respectively. The limit cycle experiment was done with this relay tuner at the point where the input servo pressure $p_1^{sv} = 2.5$ bar and the temperature 70° C. The PID parameters then, obtained from the experimental data and the algorithm in Appendix-A were :

$$K_p = -7.7143e-02, K_i = -5.7359e+00,$$
$$K_d = -2.5976e-04 \quad (8)$$

The corresponding PID controller is denoted as K_{pid}. The singular values plot of the closed loop system is shown in Fig. 14. The maximum singular values are larger than 1 everywhere. In fact, it can be calculated using the algorithm of [8] that $\|G_c\|_\infty = 260(> 1)$. The μ plot of the closed loop system is shown in Fig. 15. The maximum lower bound of μ is 1.4643, so $\|G_c\|_\Delta > 1$. These results show that this PID controller settings can not guarantee the stability and/or performance robustness in the H_∞ norm sense and in μ sense as both $\|G_c\|_\infty$ and $\|G_c\|_\Delta$ are larger than one.

B. H_∞ Control

For H_∞ control design, the following conditions have to be satisfied [9]: (1) (A, B_w) and (A, B_u) are stabilizable; (2) (C_z, A) and (C_y, A) are detectable; (3) D_{zu} has full column rank; (4) D_{yw} has full row rank. From the open loop system matrices A, B, C, and D in Section IV, these conditions can be easily checked: All eigenvalues of A are in the left half plane. The matrix pairs (A, B_w) and(A, B_u) are stabilizable, and (C_z, A) and (C_y, A) are detectable. D_{zu}, $[1\,0\,0\,0\,0\,0\,0\,0\,0\,0\,0]^T$, and D_{yw}, $[0\,0\,0\,0\,0\,0\,0\,0\,0\,1\,0]$, have full rank. An H_∞ controller, denoted as K_∞ is designed by the algorithm in [9]. It is of order 7, which is the same as the order

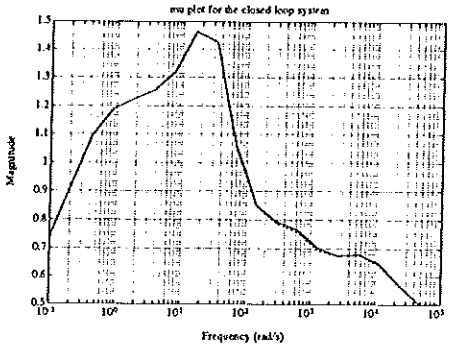

Fig. 15. μ plot of the closed loop system G_c with PID controller K_{pid} with $K_p = -7.7143e-02$, $K_i = -5.7359e+00$, $K_d = -2.5976e-04$. The solid curve is for the upper bound and the dashed curve is for the lower bound.

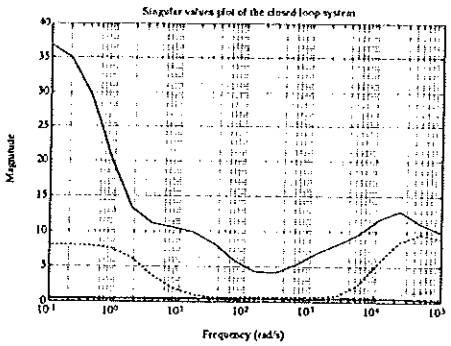

Fig. 16. Singular value plot of closed loop system with the H_∞ controller K_∞.

of plant G. The singular value plot of the closed loop system G_c is shown in Fig. 16. $\|G_c\|_\infty$ is equal to 37.5. The μ plot is shown in Fig. 17. The maximum lower bound of μ is 27.848, that is $\|G_c\|_\Delta > 1$. Both $\|G_c\|_\infty$ and $\|G_c\|_\Delta$ are larger than 1. Thus the closed loop robust stability and/or performance may not be guaranteed with such a controller.

C. μ Control Synthesis: D–K Iteration

The D–K iteration method, see Appendix-B, was used to design a controller. In each iteration step, the frequency response of the scaling factor $D(j\omega)$ is evaluated at some specified frequency points ω_i. As a result, in each iteration, a set of matrices of $D(j\omega_i)$ is found instead of the function $D(j\omega)$. To obtain $D(j\omega)$, these matrices are fit with some real, rational, minimum phase stable transfer matrices with specified orders, see [4] for detail. A second order transfer function matrix (with each entry being a second order transfer function) fit was used in each iteration for each block. In general, the higher the order of fitting, the more accurate it will be. However, for high order functions, there may be numerical problems and, typically, it results in high order controllers. Even with second order fitting, the resulting controller will be of order 39. (The scaled open loop system is DGD^{-1}, D is $\mathrm{diag}(d_1\, d_2\, d_3\, d_4\, d_5\, d_6\, d_7\, d_8\, d_9\, 1)$ with $d_i, i = 1 \cdots 8$ being second order transfer functions and d_9 equal to 1, G is of order 7, thus the scaled open loop system DGD^{-1} is of order 39 which is equal to the order of the controller). After 12 D–K iterations, a controller denoted as K_μ is found with the

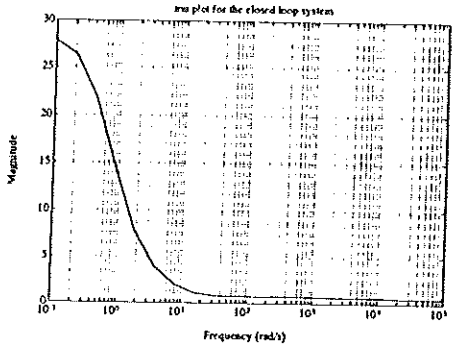

Fig. 17. μ plot of the closed loop system with the H_∞ controller K_∞. The solid curve is for the upper bound and the dashed curve is for the lower bound.

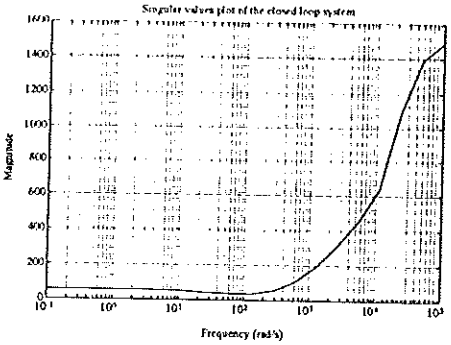

Fig. 18. Singular value plot of the closed loop system with the controller K_μ from D–K iteration.

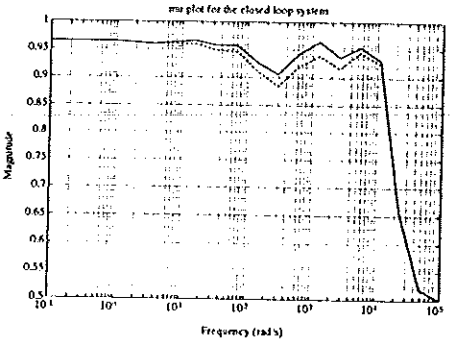

Fig. 19. μ plot of the closed loop system with the controller K_μ from D–K iteration. The solid curve is for the upper bound and the dashed curve is for the lower bound.

maximum of μ less than 1. Fig. 18 shows the closed loop system singular value plot with the controller K_μ from D–K iteration. $\|G_c\|_\infty$ is 1492 ($\gg$ 1). The μ plot is shown in Fig. 19. The maximum upper bound of μ is 0.96618, that is $\|G_c\|_\Delta < 1$, so both stability and performance robustness are guaranteed for the closed loop system with such a controller, though $\|G_c\|_\infty$ is much larger than 1. The conservativeness of the singular value test is obvious.

However, with such a high order, the controller can not be implemented in practice. A controller order reduction is definitely needed. Here we use a balanced realization model reduction method [10]. This will result in an iterative procedure. First, reduce the controller order to first order. If the μ test is satisfied, then stop, otherwise reduce the controller to second order and so on until the μ test is satisfied. By such

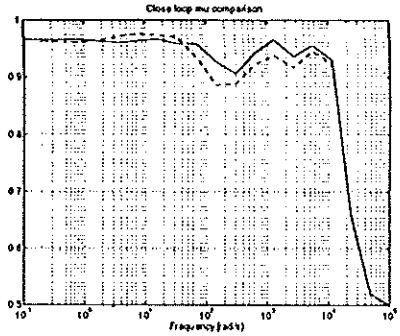

Fig. 20. Comparison of μ upper bound plots of the closed loop system G_c with the 39th order controller K_μ (dotted line) from D–K iteration and its reduced (sixth) order controller K_μ^{red} with a balanced reduction (solid line).

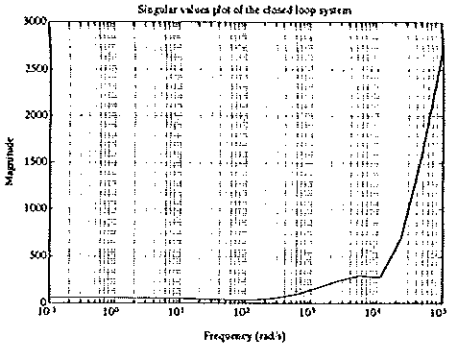

Fig. 21. Singular value plot of the closed loop system G_c with the PID controller K_{pid}^{μ} with $K_d = -3.8964e-3, K_p = -6.6808e-01$, $K_i = -9.0693e+00$.

an order reduction procedure, a sixth order controller, denoted as K_μ^{red} is obtained (The controllers of lower order obtained by this way were not stabilizing). The μ plot of the closed loop system with the order reduced controller is shown in Fig. 20. The maximum upper bound of μ is 0.979, $\|G_c\|_\Delta < 1$, while the H_∞ norm is $1492 \gg 1$.

D. PID Control 2: Parameter Space Search

From Section V-A, with the PID controller K_{pid}, μ reaches its peak value 1.4643, which is not so far from 1. To search for better PID parameters with the search method in Appendix-B, which might reduce the maximum of μ, we put a grid in the three-parameter space with the point of the values shown in (8) in the center of the grid. We used $5 \times 5 \times 5$ points with a log space interval 0.5. The minimum of the peak values of μ upper bound on these points is 1.0826 at the point:

$$K_d = -2.5976e-03, K_p = -7.7143e-01,$$
$$K_i = -1.8139e+01 \tag{9}$$

Now we do the same thing with a new grid with a center point of the values given by (9) and a smaller interval 0.12. The minimum of the peak values of μ on these new points is 0.97656 at the point:

$$K_d = -3.8964e-3, K_p = -6.6808e-01,$$
$$K_i = -9.0693e+00$$

The PID controller with these parameters is denoted by K_{pid}^{μ}. The singular value plot of the closed loop system G_c is shown in Fig. 21. The maximum singular values are larger than 1 everywhere. It can be calculated that $\|G_c\|_\infty$ is 3940($\gg$ 1). The μ plot of the closed loop system is shown in Fig. 22. The maximum upper bound of μ is 0.97656, thus $\|G_c\|_\Delta < 1$.

E. Results Comparison

All the closed loop system's characteristics with controllers designed above are summarized in Table III. The nominal closed loop system is defined by omitting all the uncertainties. Thus nominal stability is characterized by the closed loop systems poles. In all of the designs, the poles of the nominal closed loop systems are located in the left half plane, so nominal stability is guaranteed for all of them. Nominal

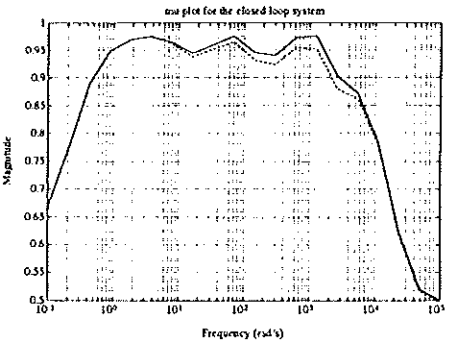

Fig. 22. μ plot of the closed loop system G_c with the PID controller K_{pid}^{μ} with $K_d = -3.8964e-3$, $K_p = -6.6808e-01$, $K_i = -9.0693e+00$. The solid curve is for the upper bound and the dashed curve is for the lower bound.

performance is characterized by the frequency responses of the nominal closed loop systems. The frequency responses for the nominal closed loop systems with different controllers are shown in Fig. 23. Nominal performance is not satisfied for the H_∞ controller K_∞ as the frequency response of the closed loop system with K_∞ is not below the specified curve ($W_p^{-1}(j\omega)$). The PID controller K_{pid} satisfies both nominal stability and performance requirements, but as discussed previously, it can't satisfy robust stability and/or performance requirements. Simulations on the original system were made for different controllers. Fig. 24 shows the simulation results of the closed loop systems with different controllers at temperature $70°C$. The input is a step signal from 40 to 20 bar. It can be seen that the best time response is that with the controller K_μ^{red} from the D–K iteration followed by the order reduction. The response with PID controller K_{pid}^{μ} is close to the best one, while the response with PID controller K_{pid} is slower. The response with the H_∞ controller is completely not acceptable.

It is difficult to see the robustness property by simulation on the original nonlinear hydraulic systems, for we don't know the exact values of the uncertainties which make the stability or performance fail. However we can show by simulation that the parameter changes may cause different effects on the time responses with different controllers. Fig. 25 shows differences between the time responses of the closed loop with PID controller K_{pid} at three different volumes of the secondary

TABLE III
SUMMARY OF DIFFERENT CONTROL DESIGNS

Controller	controller order	$\|G_c\|_\infty$	$\|G_c\|_\Delta$	robustness	nominal stability	nominal performance
K_{pid}	2	260	1.4643	no	yes	yes
K_∞	7	37.5	27.848	no	yes	no
K_μ	39	1492	0.96612	yes	yes	yes
K_μ^{red}	6	1492	0.97930	yes	yes	yes
K_{pid}^μ	2	3940	0.97656	yes	yes	yes

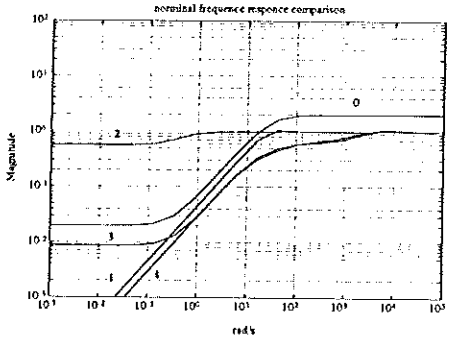

Fig. 23. Frequency responses of the closed loop system with K_{pid} (curve 1), K_∞ (curve 2), K_μ^{red} (curve 3) and K_{pid}^μ (curve 4) and the inverse of the weighting function (curve 0).

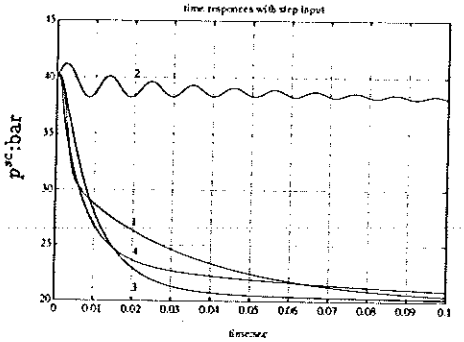

Fig. 24. Step responses of the closed loop system with K_{pid} (curve 1), K_∞ (curve 2), K_μ^{red} (curve 3) and K_{pid}^μ (curve 4).

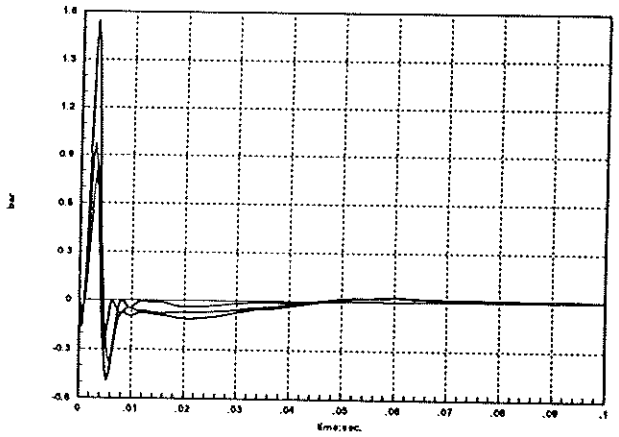

Fig. 25. The differences between the time responses with the PID controller K_{pid} with the secondary cylinder volume at 400, 280, and 160 ml.

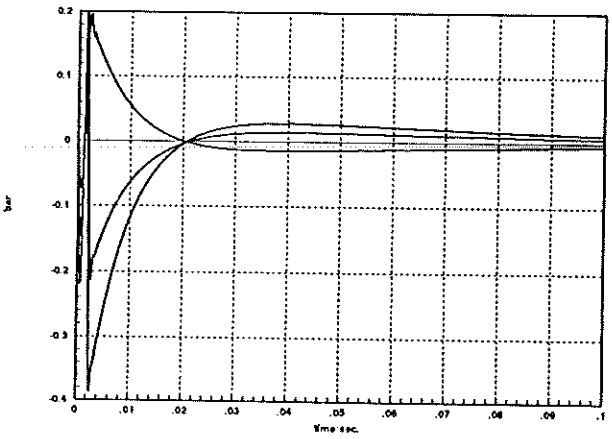

Fig. 26. The differences between the time responses with the order reduced D–K iteration controller K_μ^{red} with the secondary cylinder volume at 400, 280, and 160 ml.

cylinder. The maximum difference is 1.75 bar. Fig. 26 shows the same curves as in Fig. 25 but with K_μ^{red}. The maximum difference is 0.39 bar, smaller than 1.75. This result shows that the robustness of the closed loop with K_μ^{red} is better than that with K_{pid}.

F. Some Comments

For all of the calculations, we have used the MATLAB μ-toolbox. The current version (version 1.0) of the μ toolbox can only deal with complex block structures, while all uncertainties blocks in this paper are real scalar blocks. Thus the results here can be conservative. The μ test used here is actually the so called "frequency domain upper bound" (FDUB) test , which can be used for linear uncertainties and also for nonlinear cases when the nonlinearities are memoryless and cone bounded [11]. Here the uncertainty blocks for performance and C_c^{sc} are linear; the uncertainty blocks for G_r^{sc}, G_{r1}^{sv} and G_{r2}^{sv} are memoryless and cone bounded nonlinearities. Thus the FDUB test is valid for these uncertainty blocks. For the uncertainty blocks from C_{c1}^{sv}, C_{c1}^{sv} and G_3^{sc}, we can not guarantee that the FDUB is valid. Thus we used the so called "state space upper bound" (SSUB) test [18] to these blocks to check the results, which were all confirmed.

VI. CONCLUSION

In this paper, we have used several methods of robustness analysis and control system design for the hydraulic servo system of a CVT. The results show that the classic gain and phase margin test and PID control design can not guarantee stability and/or performance robustness. The singular value

test is rather conservative, actually it can not be used in this specific analysis problem, as the H_∞ (sub)optimal control shows that the lowest H_∞ norm of the closed loop system is 37.5, which is much larger than the required values (< 1). This means that no controller can satisfy the requirement of both stability and performance by the singular value test. The results show that in this application the upper bound of the μ test is not so conservative as the singular value test. The D–K iteration method gave a controller satisfying the robustness requirement, but its order is 39. An order reduction procedure was introduced. The lowest order of a robust controller obtained in this way is 6. Finally by locally searching in the PID parameter space, a PID controller was found such that closed-loop robustness is guaranteed. Actually it is the best controller for our practical application because of its simple structure. In addition, two procedures of uncertainty modeling were introduced for two different plant descriptions: block diagrams and transfer functions. Both of them are simple and easy to be used in practice. One remaining question is about modeling the errors from the nonlinearities. In the case of G_r^{sc}, the parameter g in the linear model is time varying and not bounded. In the case of G_{r3}^{sv}, the parameters g_x and g_p are time varying and bounded, but their range is very large. All assumptions made for these two cases are rather tricky. Verifications for the control designs based on these assumptions were made by simulation only. Another problem is that in modeling and control design, we omitted all the dynamics of electrical hydraulic actuator (PWM valve). Measurements show that in low temperature ($< 0°C$), the dynamics of PWM valve can not be neglected. Modeling these dynamics and control design for the hydraulic system with the actuator included is still underway, with the same methods presented in this paper. The real time test was done for open loop system which can only verify the system model. The real time closed loop test, to verify the control designs, is still to be made. The test is going to be done in the near future when some test facilities will be available.

Appendix
Overview of Robustness Analysis and Control System Design

In this paper, three robustness analysis methods together with their corresponding control system design methods are used. Among them, classical gain and phase margin test, singular value test based on the small gain theorem [12], [13] and H_∞ control [9] are rather standard. In this appendix, some brief overview will be made on auto-tuning PID control and μ analysis and synthesis.

A. Auto-tuning PID Control

A PID controller has a transfer function of the form:

$$K_{pid}(s) = K_p + \frac{K_i}{s} + \frac{K_d s}{T_d s + 1}$$

where K_p, K_i and K_d are parameters to be tuned. Note that the structure of a PID controller is determined a priori, irrelevant of the process to be controlled. It is different from LQG and

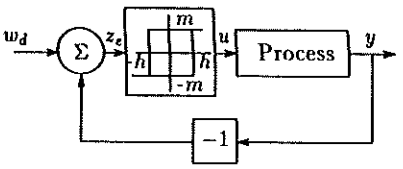

Fig. 27. An auto-tuner with a hysteresis relay.

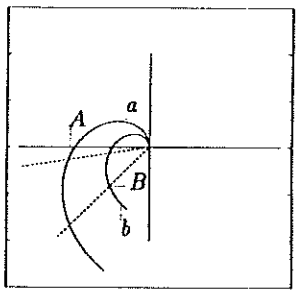

Fig. 28. Amplitude and phase margin specification.

H_∞ control designs where the controller's structures are based on the processes. The PID tuning used here is based on the specification of gain and phase margins. To do so, the limit cycle method (LCM) is used with a hysteresis relay controller to generate oscillations (see Fig. 27), so that one point in the Nyquist curve can be determined [14]. When one point on the Nyquist curve is known, it is straightforward to find the parameters of a PID regulator which give the desired amplitude and phase margins. Fig. 28 shows the gain and phase margin specification where curve a denotes the Nyquist plot of $G(j\omega)$ and curve b that of $(K_p + j\omega K_d + K_i/j\omega)G(j\omega)$ respectively. We choose the gain and phase margins so that the Nyquist plot intersects the circle with a radius 0.5 at an angle 225°. To do so, we should move the point $G(j\omega_n)$ (A in Fig. 28, ω_n is the oscillation frequency) to the point $0.5\underline{/225°}$ (B in Fig. 28). That means

$$(K_p + j\omega_n K_d + \frac{K_i}{j\omega_n})G(j\omega_n) = 0.5\underline{/225°}. \qquad (10)$$

$G(j\omega_n)$ can be rewritten in terms of gain A_g and phase ϕ_g as $G(j\omega_n) = A_g\underline{/\phi_g + 180°}$. By solving (10) for K_p, K_d and K_i, we obtain:

$$K_p = \frac{0.5\cos(45° - \phi_g)}{A_g}$$

$$K_d = K_p \frac{\tan(45° - \phi_g) + \sqrt{\frac{4}{p} + \tan^2(45° - \phi_g)}}{2\omega_n}$$

$$K_i = \frac{K_p^2}{pK_d}.$$

Here p is set to 4, which is implied in the Ziegler and Nichols tuning rule [15].

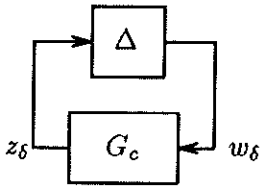

Fig. 29. Two systems connected in feedback loop to explain the small μ theorem.

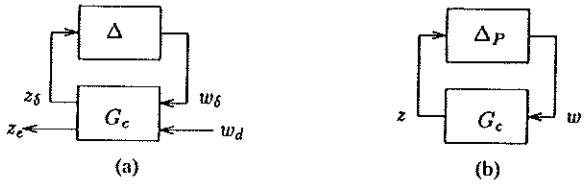

Fig. 30. The LFT of a system with uncertainty feedback.

B. Structured Singular Value Test and Synthesis

1. Definition: We adopt the definition of [16]: Given a matrix $M \in C^{n\times n}$, and a block structure $\mathbf{\Delta}$ (a set of allowed perturbation matrices), defined as:

$$\mathbf{\Delta} = \{\text{blockdiag}(\delta_1^c I_{k_1}, \cdots, \delta_{m_c}^c I_{k_{m_c}}, \Delta_1^C, \cdots, \Delta_{m_C}^C):$$

$$\delta_i^c \in C, \Delta_i^C \in C^{k_{m_c+i}\times k_{m_c+i}}, \sum_{i=1}^{m_c+m_C} k_i = n\}$$

where k_i, $i = 1, \cdots m_c + m_C$, are positive integers. The tructured singular value, $\mu_\Delta(M)$, of the matrix M with respect to the block structure $\mathbf{\Delta}$ is defined as:

$$\mu_\Delta(M) = \frac{1}{\min\{\bar\sigma(\Delta) : \Delta \in \mathbf{\Delta}, \det(I - M\Delta) = 0\}}.$$

If there exists no $\Delta \in \mathbf{\Delta}$ to satisfy $\det(I - M\Delta) = 0$, $\mu_\Delta(M) = 0$. Corresponding to the block structure $\mathbf{\Delta}$, the block structure matrix bs is defined as:

$$bs = \begin{bmatrix} k_1 & 0 \\ \vdots & \vdots \\ k_{m_c} & 0 \\ k_{m_c+1} & k_{m_c+1} \\ \vdots & \vdots \\ k_{m_c+m_C} & k_{m_c+m_C} \end{bmatrix}.$$

Thus if the ith row is $[k_i \;\; 0]$, then the ith block is a $k_i \times k_i$ repeated complex block ($\delta_i^c I_{k_i}$); while if the ith row is $[k_i \;\; k_i]$ then the ith block is a $k_i \times k_i$ full block (Δ_i^C). Because of the complexity of computation of μ, lower and upper bounds of μ are used, which are defined as [16]:

$$\max_{Q\in\mathcal{Q}} \rho(QM) \le \mu_\Delta(M) \le \inf_{D\in\mathcal{D}} \bar\sigma(DMD^{-1}) \qquad (11)$$

where

$$\mathcal{Q} = \{Q \in \mathbf{\Delta} : Q^TQ = I_n\}$$

$$\mathcal{D} = \{\text{blockdiag}(D_1, \cdots, D_{m_c}, d_1 I_{k_{m_c+1}}, \cdots d_{m_C} I_{k_{m_c+m_C}}):$$

$$0 \le D_i = D_i^T \in C^{k_i\times k_i}, 0 \le d_i \in \mathcal{R}\}.$$

The algorithms to calculate these lower and upper bounds of μ can be found in [17].

2. Analysis: Now consider the feedback system in Fig. 29. Assume $G_c(s)$ be a stable, MIMO, transfer function of a linear system; $\mathcal{M}(\Delta)$ be the set of stable rational transfer functions with block structure $\mathbf{\Delta}$. Then the following theorem gives the stability robustness test [4]:

Let $\beta \ge 0$, the loop shown in Fig. 29 is well-posed and internally stable for all $\Delta \in \mathcal{M}(\Delta)$ with $\|\Delta\|_\infty \le \frac{1}{\beta}$ if and only if

$$\|G_c\|_\Delta := \sup_{\omega\in\mathcal{R}} \{\mu_\Delta(G_c(j\omega))\} \le \beta.$$

This is the so called "small μ theorem." We can see that the small gain theorem for linear systems is a special case of the small μ theorem when the uncertainty is not structured or $\Delta \in C^{n\times n}$. Note that the μ test is not only sufficient but also necessary, while the singular value test is sufficient only when $\mathbf{\Delta} \ne C^{n\times n}$. For performance robustness test, consider the feedback system in Fig. 30, where $z = [z_\delta^t \; z_e^t]^t$, $w = [w_\delta^t \; w_d^t]^t$, and

$$\mathbf{\Delta}_P := \left\{ \begin{bmatrix} \Delta & 0 \\ 0 & \Delta_F \end{bmatrix} : \Delta \in \mathbf{\Delta}; \Delta_F \in C^{n_{z_e}\times n_{z_d}} \right\}.$$

Then the following theorem describes the μ test for stability and performance [4]:

Let $\beta \ge 0$, for all $\Delta \in \mathcal{M}(\Delta)$ with $\|\Delta\|_\infty \le \frac{1}{\beta}$. The loop shown in Fig. 30(a) is well-posed, internally stable, and $\|F_u(G_c, \Delta)\|_\infty \le \beta$ if and only if

$$\|G_c\|_{\Delta_P} := \sup_{\omega\in\mathcal{R}} \{\mu_{\Delta_P}(G(j\omega))\} \le \beta$$

Note again that this test is a necessary and sufficient condition for both stability and performance robustness, and is therefore completely nonconservative. While the singular value test is only a sufficient condition and therefore is conservative for $\mathbf{\Delta_P} \ne C^{(n+n_{z_e})\times(n+n_{w_d})}$.

3. Synthesis: D–K Iteration: From the discussion above, we need small values of $\|G_c\|_\Delta$ (we have dropped the subscript P for Δ_P) for stability and performance robustness. The μ synthesis problem is to find a stabilizing controller K that solves:

$$\min_{K \text{ stabilizing}} \|F_l(G, K)\|_\Delta.$$

Because of the computational complexity of μ, instead of minimizing $\|F_l(G, K)\|_\Delta$, we minimize on upper bound for it. That is:

$$\min_{\substack{K \text{ stabilizing} \\ D \text{ minphase,stable,} D(j\omega)\in\mathcal{D}}} \|DF_l(G, K)D^{-1}\|_\infty. \qquad (12)$$

Unfortunately it is not known how to solve this problem either as it is not a convex minimization problem. The D–K iteration method was introduced by Doyle [4] as an approximation to solve the problem. The basic idea is following: If we fix the scaling factor D, (12) is

$$\min_{K \text{ stabilizing}} \|DF_l(G, K)D^{-1}\|_\infty.$$

It is just a H_∞ synthesis problem, so it can be solved. Then if we fix the controller matrix K, (12) is

$$\min_{D \text{ minphase,stable},D(j\omega)\in\mathcal{D}} \|DF_l(G,K)D^{-1}\|_\infty.$$

It is just a problem for calculating the μ upper bound which is a convex minimization problem. Note that D–K iteration can not be guaranteed to converge to a global minimum, so if one failed to find a controller satisfying the μ test, it does not mean that there does not exist such a controller at all. The disadvantage of the D–K iteration method is the high order of a controller as a result of introducing D scaling factors in the design procedure.

4. Synthesis: PID Parameters Search: PID controllers are frequently used in industry because of their simple structure and operator's intuitive understanding of them. The natural question is whether PID control parameters (K_p, K_i and K_d) can be tuned so that the μ (or its upper bound) stability and performance test can be satisfied. The problem can be posed as follows:

$$\min_{K_p,K_i,K_d\in\mathcal{R},\ K_{pid} \text{ stabilizing}} \|F_l(G,K_{pid})\|_\Delta$$

or in the upper bound form:

$$\min_{\substack{K_p,K_i,K_d\in\mathcal{R},\ K_{pid} \text{ stabilizing} \\ D \text{ minphase,stable},D(j\omega)\in\mathcal{D}}} \|DF_l(G,K_{pid})D^{-1}\|_\infty.$$

Again this is not a convex minimization problem, so there is no attractive way to solve it. Here we search locally in the parameter space to find suitable parameters as follows. First, (1): take the initial point in the parameter space with the PID parameter values tuned based on the gain and phase margin method discussed in Appendix-A. Then (2): grid the parameter space around the initial point in, for example, $5 \times 5 \times 5$ points, (3): calculate the peak values of μ over frequency at all points. (4): If the smallest peak value of μ is less than the specified value γ then stop. Otherwise (5) regrid the parameter space with smaller intervals between points around the point with smallest peak μ calculated so far, and then go to step (3). In this way we don't need a search over all parameter space, but again, there is no guarantee to find the minimum. However, this method works in an application of the control design as shown in section V.D

ACKNOWLEDGMENT

The authors wish to thank their colleagues Paul Vanvuchelen and Willem Minten for many helpful discussions.

REFERENCES

[1] W. Minten and P. Vanvuchelen, "Modeling and simulation of an electronically controlled variable transmission," Master's Thesis, Departement Electrotechniek, K.U. Leuven, Belgium, 1991, in Dutch.
[2] *MATRIX $_X$ SYSTEM BUILD User's Guide.* Integrated System Inc., 1990.
[3] D. C. Karnopp and R. C. Rosenberg, *System Dynamics: A Unified Approach.* New York: Wiley, 1975.
[4] G. J. Balas, J. C. Doyle, K. Glover, A. Packard, and R. Smith, *μ-Analysis and Synthesis Toolbox.* The Math Works, Inc., 1991.
[5] S. Boyd and C. Barratt, *Linear Controller Design.* Englewood Cliffs, NJ: Prentice Hall, 1991.
[6] C. Yi, B. L. R. De Moor, "A multidimensional realization algorithm for parametric uncertainty modeling and multiparameter margin problems," ESAT-SISTA Rep. 1992 no. 50, Department of Electrical Engineering, K.U. Leuven, Belgium. To appear in *Int. J. Contr.*
[7] M. Steinbuch, J. C. Terlouw, O. H. Bosgra, and S. G. Smit, "Uncertainty modeling and structured singular-value computation applied to an electromechanical system," *Inst. Elect. Eng. Proc.*, vol . 139, pt. D, no. 3, pp. 301–307, May 1992.
[8] S. Boyd and V. Balakrishnan, "A regularity result for the singular values of a transfer matrix and a quadratically convergent algorithm for computing its L_∞-norm," *S yst. Control Letters*, vol. 15, no. 1, 1990.
[9] J. C. Doyle, K. Glover, P. P. Khargonekar, and E. A. Francis, "State space solutions to standard H_2 and H_∞ control problems," *IEEE Trans. Automatic Control*, vol. 34, Aug. 1989.
[10] B. C. Moore, "Principal components analysis in linear systems: Controllability, observability and model reduction," *IEEE Trans. Automatic Control*, vol. AC-26, pp 17–31, Jan. 1981.
[11] M. G. Safonov, "Stability of interconnected systems having slope bounded nonlinearities," in *6th Int. Conf. Analysis and Optimization of Systems*, Nice, France, 1984, pp. 275–287.
[12] D. A.Desoer and M.Vidyasagar, *Feedback Systems: Input-Output Properties.* New York: Academic Press, 1975.
[13] J. Doyle and G. Stein, "Multivariable feedback design: Concepts for a classical/modern synthesis," *IEEE Trans. Automatic Control*, vol. 26, pp 4–16, Jan. 1981.
[14] K. J. Åström *et al.*, "Automatic tuning of simple regulators with specifications on phase and amplitude margins," *Automatica*, vol. 30, pp. 645–651, 1984.
[15] K. J. Åström, and B. Wittenmark, *Adaptive Control.* Reading, MA: Addison-Wesley, 1989.
[16] J. Doyle, "Analysis of feedback systems with structured uncertainties," *Inst. Elect. Eng. Proc.*, vol. 129, pt. D, no. 6, pp. 242–250, Nov. 1982.
[17] A. Packard and J. C. Doyle, "The complex structured singular value," *Automatica*, vol. 29, no. 1, pp. 71–109, 1993.
[18] J. C. Doyle, A. Packard, and K. Zhou, "Review of LFT's, LMI's, and μ," in *Proc. 30th CDC*, Brighton, U.K., Dec. 1991, pp 1227–1232.



Yi Cheng received the B. S. and M. S. degrees in electrical engineering in 1982 and 1984 respectively, from Southeast University, Nanjing, China. Since 1989, he has been working towards the Ph. D. degree at the Katholieke Universiteit Leuven, Belgium.

He was a lecturer at Southeast University from 1984 to 1989 in the area of power systems.



Bart L. R. De Moor (M'86–SM'93) received the doctoral degree in applied sciences in 1988 from the Katholieke Universiteit Leuven, Belgium.

He was a visiting research associate (1988–1989) at the Department of Computer Science and Electrical Engineering of Stanford University, CA. Since October 1989, he is a senior research associate of the National Fund for Scientific Research of Belgium (NFWO) and associate professor at the Department of Electrical Engineering of the Katholieke Universiteit Leuven. In 1991–1992 he was the Chief of Staff of the Belgian National Minister of Science Wivina Demeester-DeMeyer.

Dr. De Moor received the Leybold-Heraeus Prize (1986), the Leslie Fox Prize (1989), the Guillemin-Cauer Best Paper Award (1990) of the IEEE TRANSACTIONS ON CIRCUITS AND SYSTEMS and became a Laureate of the Belgian Royal Academy of Sciences (1992).